

Contents lists available at ScienceDirect

Journal of Non-Crystalline Solids

journal homepage: www.elsevier.com/locate/jnoncrysol



Heterogeneous microstructure of Zr₄₆Cu₄₆Al₈ nanoglasses studied by quantifying glass-glass interfaces



S.D. Feng^{a,*}, L. Li^b, Y.D. Liu^a, L.M. Wang^{a,*}, R.P. Liu^a

- ^a State Key Laboratory of Metastable Materials Science and Technology, and College of Materials Science and Engineering, Yanshan University, Qinhuangdao 066004, China
- ^b Department of Metallurgical and Materials Engineering, The University of Alabama, Tuscaloosa, AL 35487, USA

ARTICLE INFO

Keywords:
Metallic glass
Interface microstructure
Molecular dynamics simulation

ABSTRACT

Heterogeneous microstructure of $Zr_{46}Cu_{46}Al_8$ nanoglasses was studied by molecular dynamics simulation. Glass-glass interfaces in nanoglasses could be told apart by formulating a contrast in the number of the quasi-nearest atom. Compared to other short-range order analysis, the quasi-nearest atom can reflect the deviated densely packing atomic clusters at the glass-glass interfaces directly. In terms of geometric and chemical short-range order, the low local fivefold symmetry and chemical segregation of interfaces improve the structural heterogeneity of nanoglasses. The local deformation preferentially takes place at the interfaces with a larger number of quasi-nearest atoms, achieving local plastic deformation tuned visually at the glass-glass interfaces. The correlation between structural and deformation properties is quantitatively assessed by tuning glass-glass interfaces. It is envisioned that the interfaces, as weak regions, can be a critical defect to tune the heterogeneous microstructure of nanoglasses.

1. Introduction

Brittle fracturing severely limits the application of metallic glasses (MGs) as structural materials [1–4]. The introduction of heterogeneous interfaces into MGs can avoid the formation of penetrating shear bands and improve the deformability of MGs [5–9]. Nanoglasses, as a new class of noncrystalline materials, possess amorphous grains surrounded by glass-glass interfaces that are in analogy to the grain boundary in polycrystalline materials [10,11]. The heterogeneous microstructure enables nanoglasses to possess excellent mechanical and functional properties that are difficult to achieve in monolithic MGs [12–14]. Notably, the glass-glass interface containing excess free volume offers a kind of structural defects that could be tailed thermodynamically and chemically to further realize the regulation of mechanical properties of amorphous materials [15,16]. For example, Fang et al. found that annealing temperature can adjust the width of the glass-glass interfaces in $Sc_{75}Fe_{25}$ nanoglasses [17].

Recently, experiments mainly focus on the characterization of the existence and width of the interfaces [17–19]. Through small-angle x-ray scattering and positron annihilation spectroscopy, interfacial regions of $\mathrm{Sc_{75}Fe_{25}}$ nanoglasses are characterized by widths of 0.8-1.2 nm [17]. Chen et al. found that the width of interfaces is 2-3 nm in magnetron sputter-deposited Au-based nanoglasses by transmission electron

microscopy (TEM) [20]. Thus, direct structural characterization of glass-glass interfaces is desirable but challenging. This is fundamentally due to the limitation of applying diffraction technique and theory, which are largely developed for crystalline materials, to the glass structure, not to mention, a few nanometers glassy interface. Advanced characterization techniques, such as state-of-the-art TEM or atom probe tomography, can provide atomic-scale resolution of structure and chemistry, and yet to capture the evolution of glass-glass interface requires further explorations [21–23].

In recent years, a few models have been used to study the nanoscale interfaces [24–28]. By molecular dynamics (MD) simulations, glass-glass interfaces with an excess free volume in a $Cu_{64}Zr_{36}$ nanoglass play a role similar to shear bands in pre-deformed MGs [25]. In a $Cu_{64}Zr_{36}$ nanoglass model, the width of glass-glass interfaces is approximately 2 nm, and the fraction of icosahedra in the interface is roughly 30% of that in the $Cu_{64}Zr_{36}$ MG counterpart [29]. Under uniaxial tensile loading of $Cu_{64}Zr_{36}$ nanoglass models, concentrated shear deformation is weakened by the formation of multiple nucleation positions of incipient shear bands [30,31].

MD simulations were performed in this work to characterize the microstructure of glass-glass interfaces in a model $\rm Zr_{46}Cu_{46}Al_8$ nanoglass. Particularly, the glass-glass interfaces were identified using the quasi-nearest atom (QNA), which is keen to atomic packing density

E-mail addresses: shidongfeng@ysu.edu.cn (S.D. Feng), limin_wang@ysu.edu.cn (L.M. Wang).

^{*} Corresponding authors.

Table 1The number and average diameter of grains in different nanoglasses.

Label	NG1	NG2	NG3
Number of grains	125	343	512
Average grain diameter (nm)	5.0 ± 0.1	3.5 ± 0.2	3.0 ± 0.2

[32–34]. The advantage of QNA on interface analysis of nanoglasses is that it can reflect atomic clusters deviating from dense-packing directly so that it is capable of distinguishing the local atomic environment by forming a contrast in the amorphous grains and glass-glass interfaces. Furthermore, the microstructure of the glass-glass interfaces including topological and chemical short-range order was characterized. A scaling relationship among peak stress, ductility and grain size was quantitatively identified. The mechanism of plastic events preferring to be initiated at interfaces was clarified.

2. Methods

The MD simulation of Zr₄₆Cu₄₆Al₈ nanoglasses used the embedded atom method (EAM) potential via LAMMPS [35,36]. Firstly, a $Zr_{46}Cu_{46}Al_8$ monolithic MG (28 nm \times 5.6 nm \times 56 nm) containing 500,000 atoms was obtained by quenching with a cooling rate of 1.0×10^{12} K/s and periodic boundary conditions (PBCs) in three directions. The Zr₄₆Cu₄₆Al₈ nanoglass was generated in the Zr₄₆Cu₄₆Al₈ monolithic MG using the Voronoi algorithm with random grain orientations through the VORONORIZE tool [37], which is a part of AtomEye utilities. And the initial $Zr_{46}Cu_{46}Al_8$ nanoglass experienced an energy minimization with a final relative energy convergence of 10^{-8} . Then the interface porosity is minimized by applying a hydrostatic pressure of 2 GPa at 50K for 0.4 ns. The sintered nanoglass was followed by the relaxation at zero pressure and 50 K for 0.4 ns. Three different nanoglasses by tuning the number of grains, and thus the grain size are listed in Table 1. These nanoglasses were subjected to uniaxial compression along the Z-direction at 4×10^7 s⁻¹ and 50 K. The Y- and Z-directions were set as PBCs, and X-direction was set as free surface. The zero pressure was applied in the Y-direction.

Based on Voronoi tessellation, each plane of Voronoi polyhedra is drawn to bisect the line connecting the center atom and its neighboring atoms [38]. The Voronoi polyhedra can be expressed by index $< n_3, n_4, n_5, n_6>$, in which n_i denotes the number of i-edged faces. By adding Voronoi index, the coordination number of the central atom can be obtained. To characterize the microstructure of nanoglasses, the pair of QNAs is adopted and three conditions need to be met at the same time

as follows [32]: (1) the pair of atoms are not nearest neighbors of each other; (2) they share a common nearest-neighbor atom; (3) their Voronoi faces of the Voronoi polyhedron centered by the common nearest-neighbor atom share an edge.

3. Results

3.1. Structural characterization

The presence of glass-glass interfaces make microstructure of nanoglasses significantly different from that of conventional MGs. However, since the microstructure of both MGs and nanoglasses are amorphous, it is difficult to characterize their differences. For example, the common number analysis (CNA) doesn't work for nanoglasses because the 'grain' and 'interface' of nanoglasses are both amorphous. Recently, a parameter called QNA is used to characterize amorphous microstructures based Voronoi polyhedra and is keen to atomic packing density [32–34]. The larger number of QNAs (N_O) represents for the looser atomic packing. Therefore, by using the N_O , the global structure of nanoglasses can be revealed clearly through formulating a contrast in the amorphous grains and glass-glass interfaces, which is similar to etching grain boundaries in polycrystalline materials. Fig. 1 shows the MG, NG I, NG II and NG III that are colored according to the N_Q . The light blue atoms with large N_Q represent glass-glass interfaces. Comparing the MG in Fig. 1a, the glass-glass interfaces of the nanoglasses in Fig. 1(b-d) are highlighted. There are some big regions in Fig. 1(b-d) that are not identified by QNA. This is because that those big grains are with similar atomic packing density, like grains in the crystal bounded by small-angle boundary. As shown in Fig. 1(b-d), the less these unidentified regions are as the number of grains increases. In other words, the probability of grains with "similar orientation" decreases as the number of grains increases, resulting in a reduction in unidentified regions.

In the following, we will analyze quantitatively the overall distribution N_Q of the nanoglasses with different gain sizes. The distribution of the N_Q in the MG, NG1, NG2 and NG3 is shown in Fig. 2. In the MGs, the atoms with $N_Q=0$, 1 and 2 dominate, while in the nanoglasses the atoms with $N_Q=1$, 2, 3, 4, 5, and 6 all become significant. Overall, the fractions of atoms with $N_Q\leq 2$ in nanoglasses gradually decrease with the reduction of grain sizes, whereas atoms with $N_Q>2$ gain popularity. It is worth noting that the population of $N_Q=4$ is greater than that of the others (except for $N_Q=0$) accounting for the main proportion in the nanoglasses. As shown in the insert, the

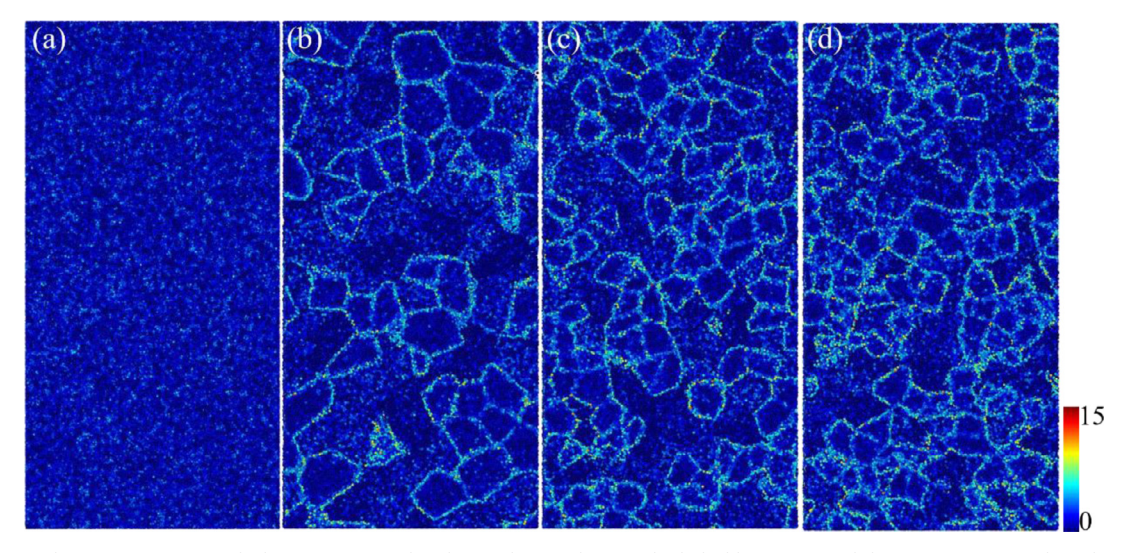


Fig. 1. The (a) MG, (b) NG I, (c) NG II and (d) NG III were colored according to the N_Q . The light blue atoms with large N_Q represent glass-glass interfaces. (For interpretation of the references to color in this figure legend, the reader is referred to the web version of this article.)

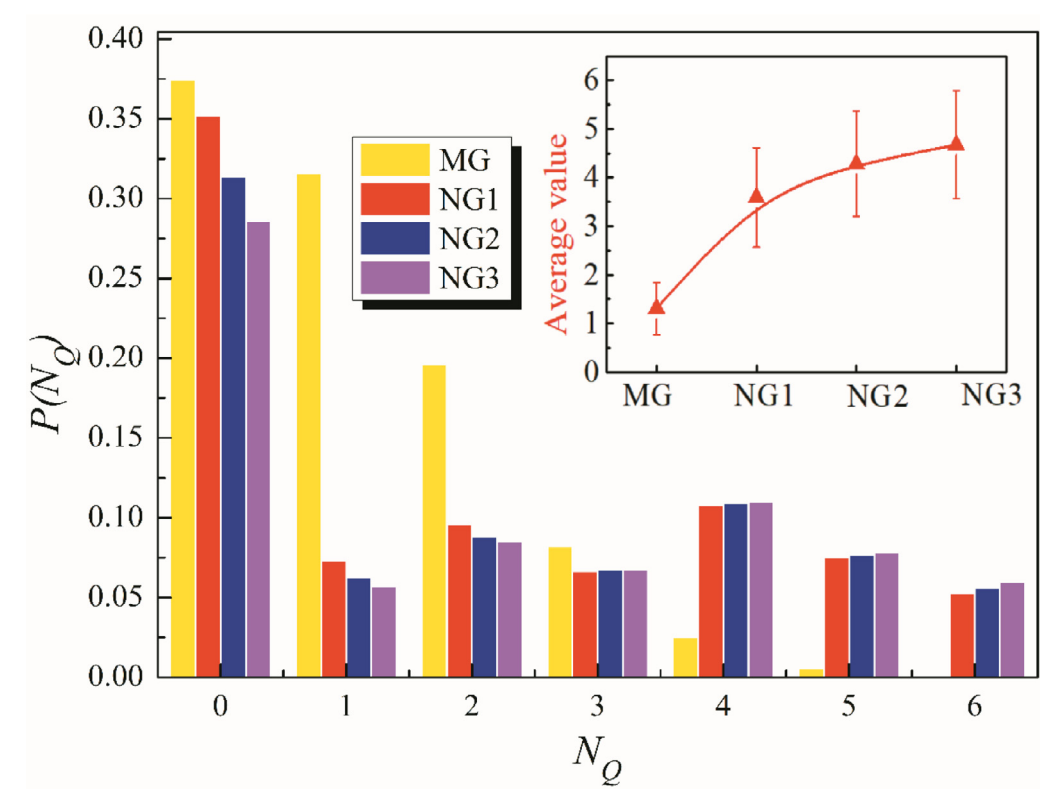


Fig. 2. The distribution of the N_O for the MG, NG1, NG2 and NG3. The insert shows the average value of N_O .

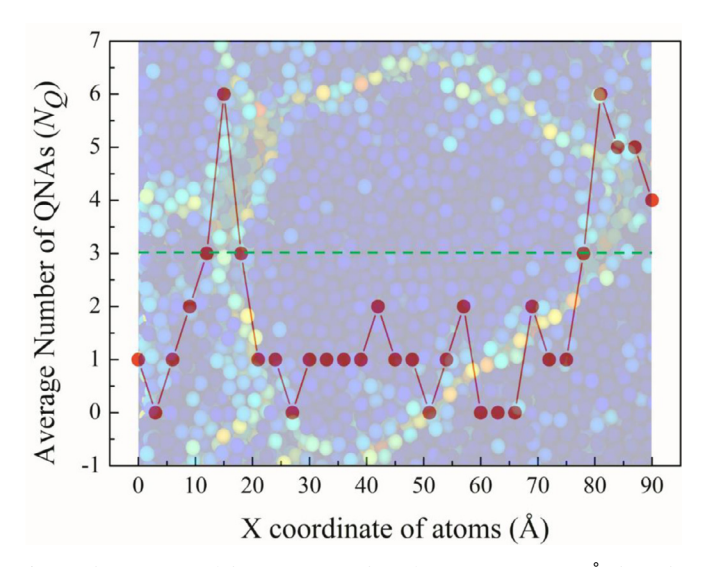


Fig. 3. The variation of the average number of QNAs (N_Q) every 3 Å along the green dotted line that crosses "grain" and "interface".

average value of the N_Q for the MG, NG1, NG2 and NG3 gradually increase with the reduction of grain sizes. The larger the N_Q around the central atom, the greater the ability of the central atom to move [34]. The above illustrates that the QNA can recognize the looser atomic packing environment induced by forming more glass-glass interfaces.

To show the grain regions and interfaces more clearly, Fig. 3 shows the variation of average N_Q every 3 Å along the green dotted line that goes through "grain" and "interface". Inside the grain, the average N_Q is about 1, which is consistent with the N_Q of MGs [32,34], while the interface's N_Q is around 6. Therefore, different grains in the nanoglasses can be distinguished by N_Q to highlight the different amorphous grains and glass-glass interfaces. Next, atoms with $N_Q \geq 6$ are identified to be the interface atoms. To characterize the topological frustration of short-

range order, Voronoi polyhedra denoted by $\langle n_3, n_4, n_5, n_6 \rangle$ were employed. During the glass transition, the proportion of pentagonal faces n_5 with five-fold symmetry increases sharply, compared to triangle, tetragon and hexagon faces with translational symmetry [39]. During deformation, the deformation units are formed in regions with lower pentagonal structures n_5 because of their higher packing density [40]. Therefore, it is essential to investigate the distribution of pentagons n_5 of polyhedra in grains and interfaces.

The fraction of pentagons n_5 in polyhedra with different coordination numbers (CN) is shown in Fig. 4a. Grid-lines represent interfaces, while solid areas represent grains. In the polyhedra with different CN, the pentagonal fraction in the grains is greater than that in the interfaces, except Voronoi polyhedra with $n_5 = 6$. The Voronoi polyhedra with $n_5 = 6$ possess low five-fold symmetry, while the Voronoi polyhedra with $n_5 = 8$, 10 and 12 possess high five-fold symmetry. Therefore, the pentagonal structures in interfaces are greatly reduced. The above quantitatively characterizes the decrease of local fivefold symmetry of interfaces, which proves the effectiveness of QNA to determine the interfaces. In addition to the topological frustration of short-range order, the chemical short-range order is also characterized. The percent of partial coordination number (PCN) for central elements Zr, Cu and Al in the grains and interfaces is shown in Fig. 4b. In the grain, the proportion of Zr, Cu and Al atoms around each central element is about 46%, 46% and 8%, which is consistent with the proportion of the Zr₄₆Cu₄₆Al₈ monolithic MG; While in the interfaces, the proportion of Zr atoms around each central element is greatly decreased, and the proportion of Al atoms around each central element increases significantly. The average chemical composition of interfaces is Zr₃Cu₄₁Al₅₆, suggesting pronounced chemical segregation at the interfaces. It is worth noting that the preparation of nanoglasses in this work is at 50 K, and increasing the preparation or annealing temperatures can enhance mobility of atoms and further change the interfacial chemistry, which will be explored in the future. It is envisioned that the interfaces, as weak regions, can be a critical defect to tune the heterogeneous microstructure of nanoglasses.

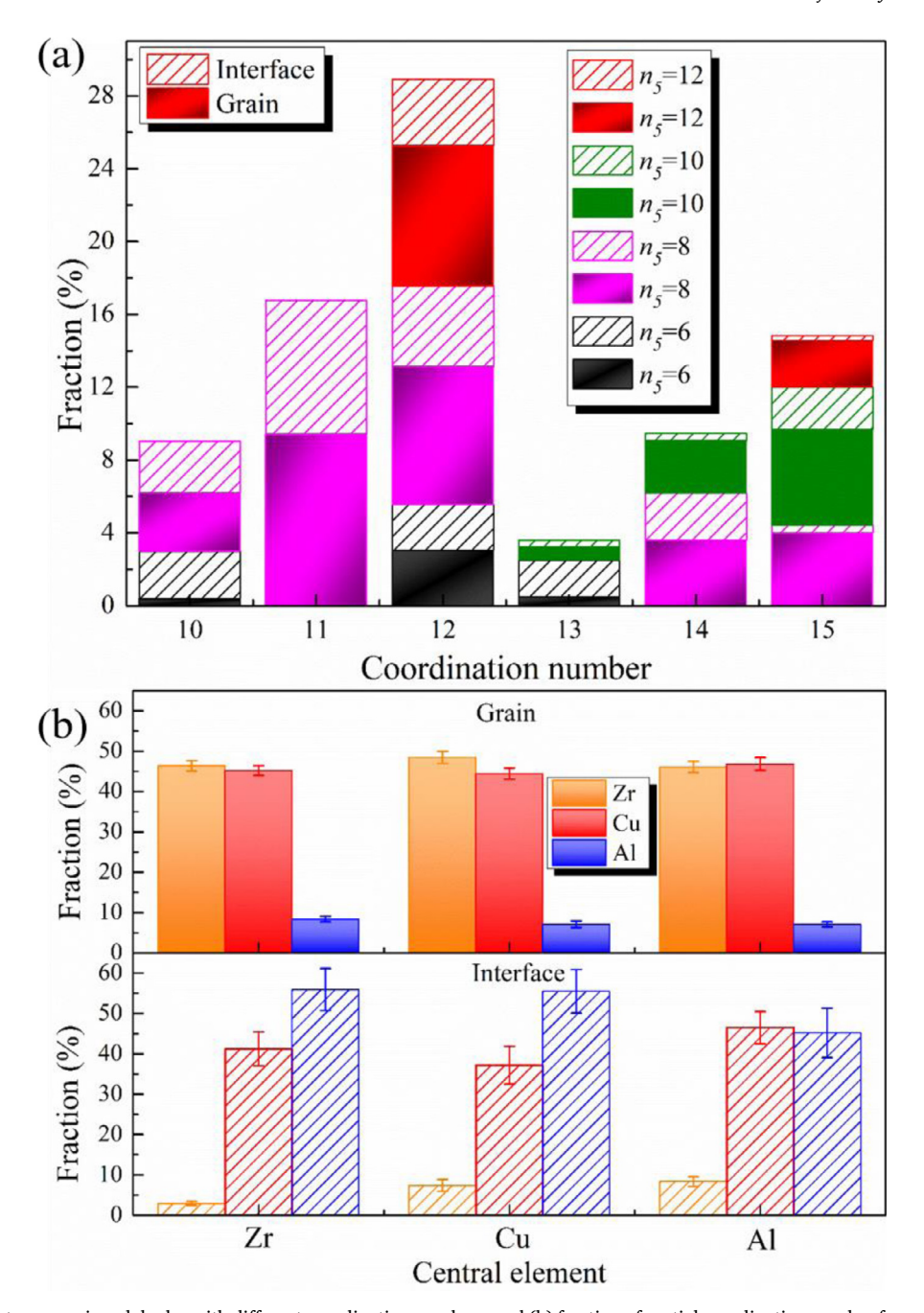


Fig. 4. (a) Fraction of pentagons n_5 in polyhedra with different coordination numbers, and (b) fraction of partial coordination number for central elements Zr, Cu and Al at "grain" and "interface" of the nanoglasses.

3.2. Compression tests

The simulation results above clearly show the glass-glass interfaces and their short-range order. In the following, the relationship between interfaces and QNA during deformation is discussed. The compressive stress-strain curves of different nanoglasses are shown in Fig. 5. The stress-strain curves of the nanoglasses are seriously different from that of the monolithic MG. The sudden drop after the peak stress τ_y in the monolithic MG corresponds to form penetrating shear bands [41], while that doesn't occur in the nanoglasses. After the sudden drop, the stress reaches the stable flow stress τ_s . The value of $(\Delta\tau=\tau_y-\tau_s)$ corresponds to the structural softening and strain localization [42–44]. The significant reduction of the stress drop $\Delta\tau$ for nanoglasses corresponds to the enhanced plasticity. It is worth noting that the peak stress τ_y and the flow stress τ_s can be changed by changing grain size and glass-glass

interfaces. The maximum stress of the NG1 is even greater than that of the MG. The insert shows the scaling relationship among peak stress, grain size and initial interface fraction. The interfacial fraction is obtained by roughly counting initial atoms with $N_Q \geq 6$ that can represent the interface. It is found that peak stress decreases with increasing interface fraction, and interface fraction increases with decreasing grain size. For MGs, the interfacial fraction is ~ 0 , and the fit linear curve cannot retrieve the yield stress. This is because that during deformation, the penetrating shear bands play a leading role in MGs, while the multiple glass-glass interfaces play that role in nanoglasses.

In addition to clarifying the relationship between strength and interface fraction, the relationship between plasticity and interface fraction has also been investigated. The von Mises strain $\eta^{Mises}>0.3$ is utilized to quantify the ability of atoms to participate in deformation [45–47]. Fig. 6 illustrates the proportion of atoms with $\eta^{Mises}>0.3$ as a

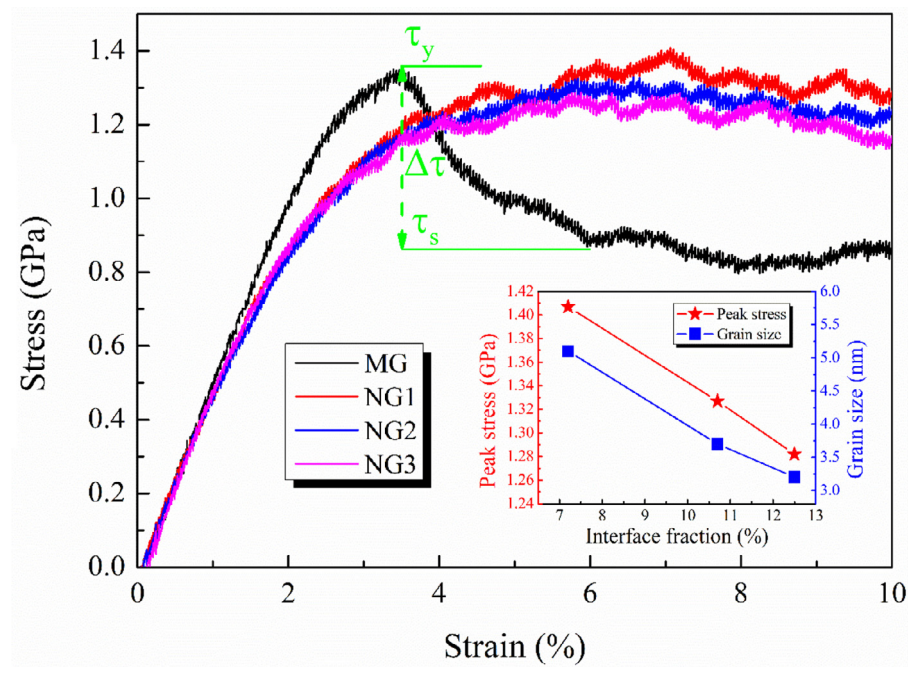


Fig. 5. Stress-strain curves of nanoglasses with different grain sizes: the MG, NG1, NG2 and NG3. The insert shows the scaling relationship among peak stress, grain size and initial interface fraction.

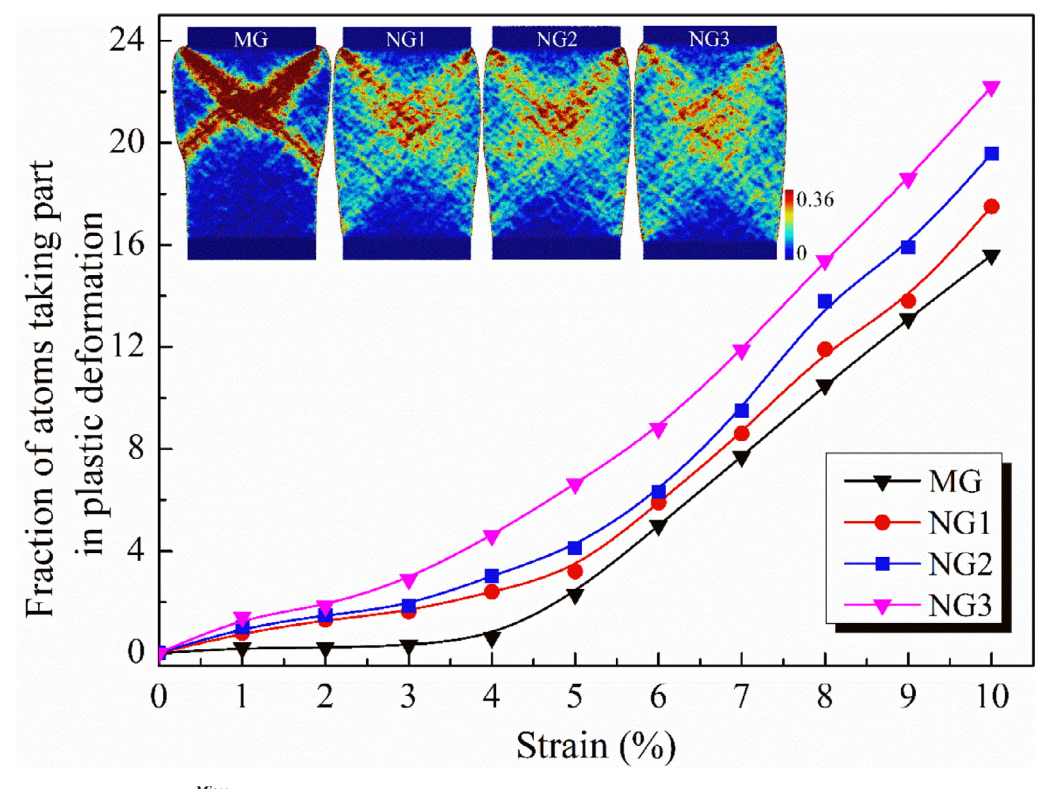


Fig. 6. The proportions of atoms with $\eta^{Mises} > 0.3$ for the nanoglasses as a function of strain. The insert shows the snapshots of models at the strain of 10%.

function of compressive strain. At the same strain, the proportion increases with decreasing grain size (increasing interfaces). For the monolithic MG, the proportion proportion radically increases after 4% strain; while for the nanogalsses, the proportion keeps increasing with strain, without monolithic-MG-like platform before 4% strain. This suggests that initial glass-glass interfaces provide nucleation positions for deformation. In the insert of Fig. 6, two penetrating shear bands form at the strain of 10% in the MG, while in the nanogalsses, tiny

deformation units are distributed throughout the samples. Adibi found that the microstructures for the shear bands and the glass-glass interfaces of nanoglasses are nearly identical [31], implying that glass-glass interfaces play the role of pre-introduced shear bands. These interfaces interact with each other, which limits the rapid propagation of a single shear band and promotes the homogeneous deformation [48]. The smaller the grain, the more the glass-glass interface, the more homogeneous the deformation. The proportion of atoms involved in plasticity

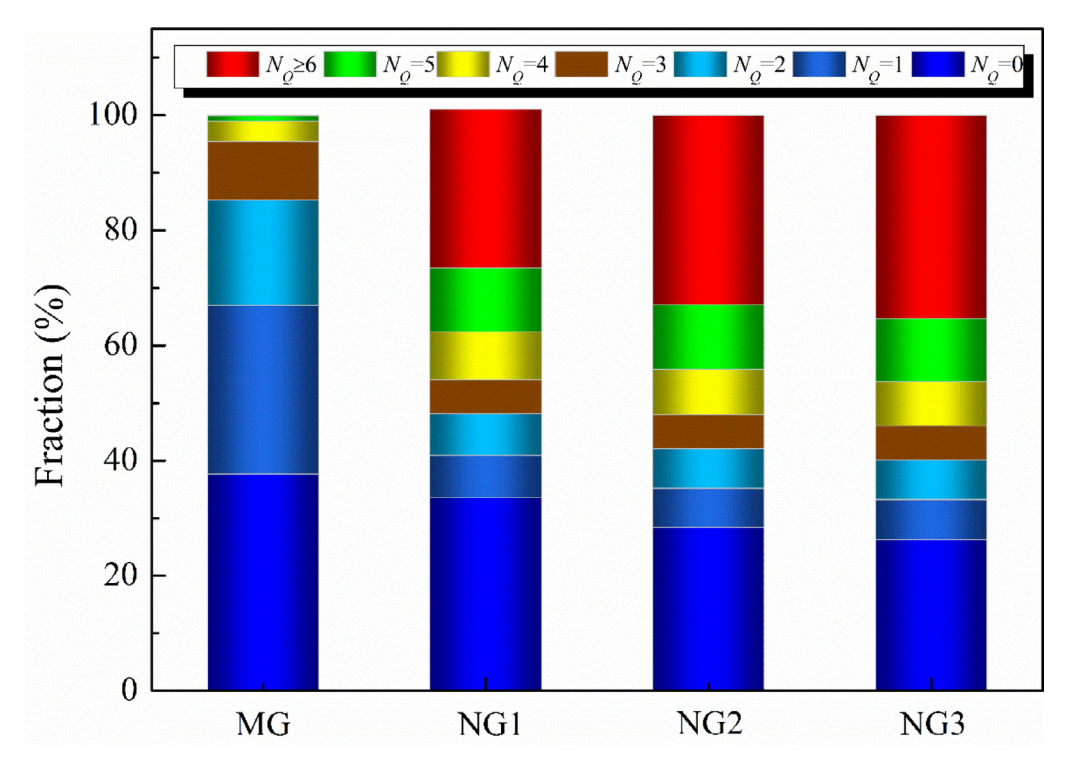


Fig. 7. The distribution of the initial N_O for atoms in the MG, the NG1, the NG2 and the NG3 before loading.

for the NG3 with maximum proportion of interfaces is largest, indicating most homogeneous deformation in these nanoglasses.

4. Discussion

Next, the parameter N_O will be regarded as a guide to explain why nanoglasses with more interfaces show enhanced plasticity. Fig. 7 shows the distribution of the initial N_Q in the MG, the NG1, the NG2 and the NG3 before loading. In the nanoglasses, the atoms with $N_Q = 0$ gradually decrease with decreasing grain sizes (increasing the glassglass interfaces). For example, the fraction of atoms with $N_Q = 0$ is the smallest for the NG3. Comparing the large fraction of the atoms with N_O = 1 or 2 in the MG, the atoms with N_Q = 1 or 2 in the nanoglasses are greatly reduced. In the MG, there is almost no atom with $N_Q \ge 6$, while in nanoglasses, the fraction of atoms with $N_Q \ge 6$ reaches 27%~35%. And the smaller the grain size, the larger the fraction of atoms with N_Q \geq 6. In the NG3, the fraction of atoms with $N_Q \geq$ 6 is largest. By comparing the MG, the NG1, the NG2 and the NG3 in Fig. 6, at the same strain, the proportion of atoms with $\eta^{Mises} > 0.3$ increases with decreasing grain size (increasing interfaces), which is the same as the change trend of $N_Q \ge 6$ in Fig. 7. Therefore, atoms with $N_Q \ge 6$ can represent the structural signal of the glass-glass interfaces. For the MG, plastic events start with small N_Q but change quite dramatically due to strain localization. For the nanoglass, deformation units prefer to be initiated in interfaces with large N_O but the change could be small due to distributed flow. This is proven by the proportions of atoms with $\eta^{Mises} > 0.3$ as a function of compressive strain in Fig. 6. For the monolithic MG, the proportion is small and basically remains the same before 4 % strain, while the proportion rapidly increases after 4% strain. For the nanogalsses, the proportion of atoms with $\eta^{\textit{Mises}} > 0.3$ keeps increasing with strain, without monolithic-MG-like platform before 4% strain. Therefore, plastic events corroborate well with initial interfaces represented by $N_O \ge 6$, and local plastic deformation can be tuned visually before loading.

5. Conclusions

The heterogeneous microstructure of a $\rm Zr_{46}Cu_{46}Al_8$ nanoglass was characterized by MD simulations. The QNA is keen to the atomic packing density and can distinguish the amorphous grains and glass-glass interfaces. The distribution of pentagons n_5 of Voronoi polyhedra quantitatively characterizes the low local fivefold symmetry of interfaces, proving the effectiveness of QNA. In addition to the geometric short-range order by Voronoi polyhedra, partial coordination number characterizes chemical segregation at the interfaces in terms of chemical short-range order. The average value N_Q gradually increase with forming more glass-glass interfaces, improving structural heterogeneity. The deformation units preferentially take place at interfaces with $N_Q \geq 6$, and atoms with $N_Q \geq 6$ can represent the structural signal of the glass-glass interfaces during deformation, achieving local plastic deformation tuned visually before loading.

CRediT authorship contribution statement

S.D. Feng: Investigation, Data curation, Software, Writing - original draft, Project administration, Funding acquisition. L. Li: Writing - review & editing, Funding acquisition. Y.D. Liu: Methodology, Validation. L.M. Wang: Project administration, Formal analysis, Funding acquisition. R.P. Liu: Validation, Supervision.

Declaration of Competing Interest

The authors declare that they have no known competing financial interests or personal relationships that could have appeared to influence the work reported in this paper.

Acknowledgements

This work was supported by the National Natural Science Foundation of China under Grant 51801174; National Key R&D Program of China under Grant 2018YFA0703602; and the Program for the Top Young Talents of Higher Learning Institutions of Hebei under

Grant BJ2018021; LL would like to acknowledge the support from the National Science Foundation under grant number CMMI 17-0267.

Supplementary materials

Supplementary material associated with this article can be found, in the online version, at doi:10.1016/j.jnoncrysol.2020.120265.

References

- J.C. Qiao, Q. Wang, J.M. Pelletier, H. Kato, R. Casalini, D. Crespo, E. Pineda, Y. Yao, Y. Yang, Structural heterogeneities and mechanical behavior of amorphous alloys, Proc. Mater Sci. 104 (2019) 250–329.
- [2] A. Rauf, C.Y. Guo, Y.N. Fang, Z. Yu, B.A. Sun, T. Feng, Binary Cu-Zr thin film metallic glasses with tunable nanoscale structures and properties, J. Non-Cryst. Solids 498 (2018) 95–102
- [3] A.L. Greer, Y.Q. Cheng, E. Ma, Shear bands in metallic glasses, Mater. Sci. Eng. R 74 (2013) 71–132
- [4] R. Limbach, K. Kosiba, S. Pauly, U. Kühn, L. Wondraczek, Serrated flow of CuZr-based bulk metallic glasses probed by nanoindentation: role of the activation barrier, size and distribution of shear transformation zones, J. Non-Cryst. Solids 459 (2017) 130–141.
- [5] Y. Wang, J. Li, A.V. Hamza, T.W. Barbee Jr, Ductile crystalline-amorphous nanolaminates, Proc. Natl. Acad. Sci. U.S.A. 104 2007, pp. 11155–11160.
- [6] Y. Jiang, Q. Wu, L. Sun, Macroscopic tensile plasticity of metallic glass matrix composites through gradient microstructures, J. Non-Cryst. Solids 475 (2017) 96–100.
- [7] S.D. Feng, L. Li, K.C. Chan, L. Qi, L. Zhao, L.M. Wang, R.P. Liu, Control of shear band dynamics in Cu₅₀Zr50 metallic glass by introducing amorphous-crystalline interfaces, J. Alloys Compd. 770 (2019) 896–905.
- [8] H.Y. Song, M. Wang, M.R. An, Y.L. Li, Enhancing the plasticity of noncrystalline CuZr multilayer: insights from molecular dynamics simulations, J. Non-Cryst. Solids 507 (2019) 11–18.
- [9] H.Y. Song, P. Yin, X.D. Zuo, M.R. An, Y.L. Li, Atomic simulations of plastic deformation mechanism of MgAl/Mg nanoscale amorphous/crystalline multilayers, J. Non-Cryst. Solids 500 (2018) 121–128.
- [10] H. Gleiter, T. Schimmel, H. Hahn, Nanostructured solids–from nano-glasses to quantum transistors, Nano Today 9 (2014) 17–68.
- [11] H. Gleiter, Nanoglasses: a new kind of noncrystalline materials, Beilstein J. Nano. Tech. 4 (2013) 517–533.
- [12] X.L. Wang, F. Jiang, H. Hahn, J. Li, H. Gleiter, J. Sun, J.X. Fang, Plasticity of a scandium-based nanoglass, Scripta Mater. 98 (2015) 40–43.
- [13] N. Chen, D. Wang, T. Feng, R. Kruk, K.-F. Yao, D.V. Louzguine-Luzgin, H. Hahn, H. Gleiter, A nanoglass alloying immiscible Fe and Cu at the nanoscale, Nanoscale 7 (2015) 6607–6611.
- [14] J.Q. Wang, N. Chen, P. Liu, Z. Wang, D.V. Louzguine-Luzgin, M.W. Chen, J.H. Perepezko, The ultrastable kinetic behavior of an Au-based nanoglass, Acta Mater. 79 (2014) 30–36.
- [15] H. Gleiter, Our thoughts are ours, their ends none of our own: are there ways to synthesize materials beyond the limitations of today? Acta Mater. 56 (2008) 5875–5893
- [16] R. Witte, T. Feng, J. Fang, A. Fischer, M. Ghafari, R. Kruk, R. Brand, D. Wang, H. Hahn, H. Gleiter, Evidence for enhanced ferromagnetism in an iron-based nanoglass, Appl. Phys. Lett. 103 (2013) 073106.
- [17] J.X. Fang, U. Vainio, W. Puff, R. Wurschum, X.L. Wang, D. Wang, M. Ghafari, F. Jiang, J. Sun, H. Hahn, Atomic structure and structural stability of Sc75Fe25 nanoglasses, Nano Lett. 12 (2011) 458–463.
- [18] M. Ghafari, S. Kohara, H. Hahn, H. Gleiter, T. Feng, R. Witte, S. Kamali, Structural investigations of interfaces in Fe90Sc10 nanoglasses using high-energy x-ray diffraction, Appl. Phys. Lett. 100 (2012) 133111.
- [19] Y. Ivanisenko, C. Kübel, S.H. Nandam, C. Wang, X. Mu, O. Adjaoud, K. Albe, H. Hahn, Structure and properties of nanoglasses, Adv. Eng. Mater. 20 (2018) 1800404.
- [20] N. Chen, D.V. Louzguine-Luzgin, G.Q. Xie, P. Sharma, J.H. Perepezko, M. Esashi, A.R. Yavari, A. Inoue, Structural investigation and mechanical properties of a representative of a new class of materials: nanograined metallic glasses, Nanotechnology 24 (2013) 045610.

- [21] H. Gleiter, Nanoglasses: a new kind of noncrystalline material and the way to an age of new technologies? Small 12 (2016) 2225–2233.
- [22] N. Chen, R. Frank, N. Asao, D. Louzguine-Luzgin, P. Sharma, J. Wang, G. Xie, Y. Ishikawa, N. Hatakeyama, Y. Lin, Formation and properties of Au-based nanograined metallic glasses, Acta Mater. 59 (2011) 6433–6440.
- [23] R. Witte, T. Feng, J.X. Fang, A. Fischer, M. Ghafari, R. Kruk, R.A. Brand, D. Wang, H. Hahn, H. Gleiter, Evidence for enhanced ferromagnetism in an iron-based nanoglass, Appl. Phys. Lett. 103 (2013) 073106.
- [24] Z.D. Sha, P.S. Branicio, Q.X. Pei, Z.S. Liu, H.P. Lee, T.E. Tay, T.J. Wang, Strong and superplastic nanoglass, Nanoscale 7 (2015) 17404–17409.
- [25] Y. Ritter, D. Şopu, H. Gleiter, K. Albe, Structure, stability and mechanical properties of internal interfaces in Cu₆₄Zr36 nanoglasses studied by MD simulations, Acta Mater. 59 (2011) 6588–6593.
- [26] K. Albe, Y. Ritter, D. Şopu, Enhancing the plasticity of metallic glasses: shear band formation, nanocomposites and nanoglasses investigated by molecular dynamics simulations, Mech. Mater. 67 (2013) 94–103.
- [27] O. Adjaoud, K. Albe, Microstructure formation of metallic nanoglasses: insights from molecular dynamics simulations, Acta Mater. 145 (2018) 322–330.
- [28] M. Zhang, Q.-M. Li, J.-C. Zhang, G.-P. Zheng, X.-Y. Wang, The prominent combination of ultrahigh strength and superior tensile plasticity in Cu–Zr nanoglass connected by oxide interfaces: a molecular dynamics study, J. Alloys Compd. 801 (2019) 318–326.
- [29] B. Cheng, J.R. Trelewicz, Controlling interface structure in nanoglasses produced through hydrostatic compression of amorphous nanoparticles, Phys. Rev. Mater. 3 (2019) 035602.
- [30] D. Şopu, Y. Ritter, H. Gleiter, K. Albe, Deformation behavior of bulk and nanos-tructured metallic glasses studied via molecular dynamics simulations, Phys. Rev. B 83 (2011) 100202.
- [31] S. Adibi, P.S. Branicio, Y.W. Zhang, S.P. Joshi, Composition and grain size effects on the structural and mechanical properties of CuZr nanoglasses, J. Appl. Phys. 116 (2014) 043522.
- [32] S.P. Pan, S.D. Feng, J.W. Qiao, W.M. Wang, J.Y. Qin, Correlation between local structure and dynamic heterogeneity in a metallic glass-forming liquid, J. Alloys Compd. 664 (2016) 65–70.
- [33] X.F. Niu, S.D. Feng, S.P. Pan, Related structure characters and stability of structural defects in a metallic glass, Materials 11 (2018) 468.
- [34] S.D. Feng, K.C. Chan, S.H. Chen, L. Zhao, R.P. Liu, The role of configurational disorder on plastic and dynamic deformation in Cu₆₄Zr36 metallic glasses: a molecular dynamics analysis, Sci. Rep. 7 (2017) 40969.
- [35] S. Plimpton, Fast parallel algorithms for short-range molecular dynamics, J. Comput. Phys. 117 (1995) 1–19.
- [36] Y.Q. Cheng, E. Ma, H.W. Sheng, Atomic level structure in multicomponent bulk metallic glass. Phys. Rev. Lett. 102 (2009) 245501.
- [37] J. Li, AtomEye: an efficient atomistic configuration viewer, Modell. Simul. Mater. Sci. Eng. 11 (2003) 173.
- [38] N. Medvedev, The algorithm for three-dimensional Voronoi polyhedra, J. Comput. Phys. 67 (1986) 223–229.
- [39] M. Wakeda, Y. Shibutani, S. Ogata, J. Park, Relationship between local geometrical factors and mechanical properties for Cu–Zr amorphous alloys, Intermetallics 15 (2007) 139–144.
- [40] H.L. Peng, M.Z. Li, W.H. Wang, Structural signature of plastic deformation in metallic glasses, Phys. Rev. Lett. 106 (2011) 135503.
- [41] A.J. Cao, Y.Q. Cheng, E. Ma, Structural processes that initiate shear localization in metallic glass, Acta Mater. 57 (2009) 5146–5155.
- [42] D. Rodney, C. Schuh, Distribution of thermally activated plastic events in a flowing glass, Phys. Rev. Lett. 102 (2009) 235503.
- [43] F. Shimizu, S. Ogata, J. Li, Yield point of metallic glass, Acta Mater. 54 (2006) 4293–4298
- [44] S.D. Feng, L. Qi, L.M. Wang, S.P. Pan, M.Z. Ma, X.Y. Zhang, G. Li, R.P. Liu, Atomic structure of shear bands in Cu₆₄Zr36 metallic glasses studied by molecular dynamics simulations, Acta Mater. 95 (2015) 236–243.
- [45] F. Shimizu, S. Ogata, J. Li, Theory of shear banding in metallic glasses and molecular dynamics calculations, Mater. Trans. 48 (2007) 2923–2927.
- [46] Z.D. Sha, Q.X. Pei, V. Sorkin, P.S. Branicio, Y.W. Zhang, H.J. Gao, On the notch sensitivity of CuZr metallic glasses, Appl. Phys. Lett. 103 (2013) 081903.
- 47] Y.Q. Cheng, A.J. Cao, E. Ma, Correlation between the elastic modulus and the intrinsic plastic behavior of metallic glasses: the roles of atomic configuration and alloy composition, Acta Mater. 57 (2009) 3253–3267.
- [48] K.V. Reddy, C. Deng, S. Pal, Dynamic characterization of shock response in crystalline-metallic glass nanolaminates, Acta Mater. 164 (2019) 347–361.